THE AMERICAN SOCIETY OF MECHANICAL ENGINEERS
Three Park Avenue, New York, N.Y. 10016-5990

99-GT-264

COMPARISON OF COMPUTATIONAL VELOCITY AND HEAT TRANSFER PREDICTIONS TO EXPERIMENTAL MEASUREMENTS IN A ROTATING COOLING PASSAGE WITH SMOOTH WALLS

Jeffrey P. Bons
Department of Aeronautics and Astronautics
Air Force Institute of Technology
Wright-Patterson AFB, OH 45433

ABSTRACT

Numerical predictions of the turbulent velocity field and wall heat transfer for a simulated turbine blade cooling passage are presented. The square cross-sectioned, smooth-walled passage is identical to one for which velocity and heat transfer data are available for comparison. Reynolds number (8000), rotation number (0.2), and buoyancy numbers (0 and 0.49) are typical of gas turbine applications. Predictions are presented for three turbulence models: standard k-ε, Renormalization Group k-ε, and Reynolds Stress. In addition, two wall treatments are evaluated: wall functions and a two-layer zonal model. Results from the three models are comparable, however the two-layer zonal wall treatment provides the best match to both the experimental flowfield data and the Nusselt distribution. Wall functions are shown to be unsuitable for this flowfield. General flow features in the passage are adequately captured by the zonal model including the Coriolis-induced double vortex and the distorted streamwise velocity profile due to the buoyancy effect. Agreement between the calculated and measured streamwise velocity profile (from leading to trailing wall) is particularly remarkable and contributes to an impressive leading and trailing Nu match with the data. This agreement suggests that the model adequately accounts for the buoyancy effect on the bulk flow without any buoyancy terms in the k or ε conservation equations. The model is less effective, however, at capturing the specific vortex position and strength. Specifically, the model vortex has only half the measured vortex maximum velocity and is located forward or aft of the passage centerline (depending on the density ratio of the flow).

NOMENCLATURE

Bo - Buoyancy param. = $\beta(T-T_{in})R_m\Omega^2 d/u_{in}^2$
d - hydraulic diameter = 1cm
d.r. - density ratio = $(T_w-T_{in})/T_w$
Gr_Ω - rotational Grashof number
k - gas thermal conductivity
  - turbulent kinetic energy
l - passage length = 11.5cm
Nu - Nusselt number = $qd/k_{film}(T_w-T_{bulk})$
Pr - Prandtl number = ν/α
q - surface heat flux
r or R - radial distance to axis of rotation
R_m - mean radius of test section
Ra_Ω - rotational Rayleigh number
Re - passage Reynolds number = du_{in}/ν
Re_y - turbulent Reynolds number
Rot - Rotation number = $\Omega d/u_{in}$
T - local static temperature
u - x component of velocity
u_{cor} – Coriolis component of u velocity
u_τ – shear velocity = $(\tau_w/\rho)^{1/2}$
v - y component of velocity
V - complete velocity vector
w - z component of velocity
x - radial (streamwise) direction in passage
y - axis parallel with axis of rotation
y^+ - dimensionless wall distance = yu_τ/ν
z - crossflow direction in passage
α - thermal diffusivity
β - volumetric expansion coefficient
ε - turbulent dissipation rate
μ - viscosity
ν - kinematic viscosity
ρ - fluid density
τ_w - wall shear
Ω - rotational frequency

Presented at the International Gas Turbine & Aeroengine Congress & Exhibition
Indianapolis, Indiana — June 7–June 10, 1999

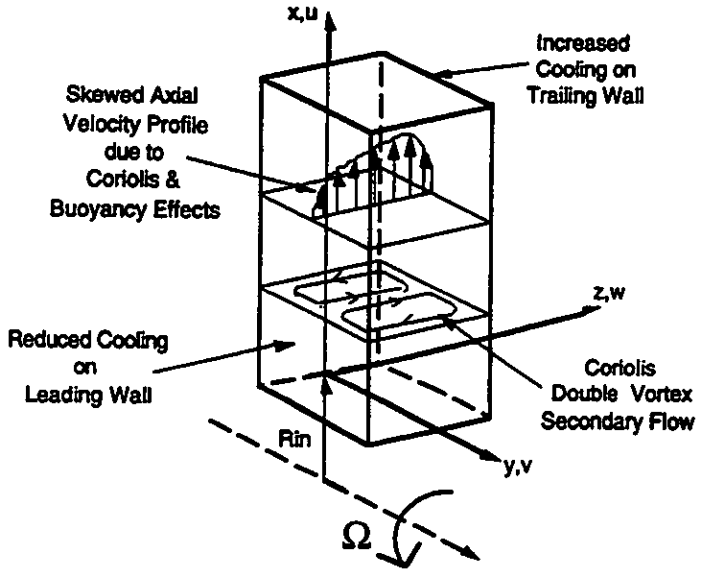

Figure 1: Schematic of Heated, Rotating Flow

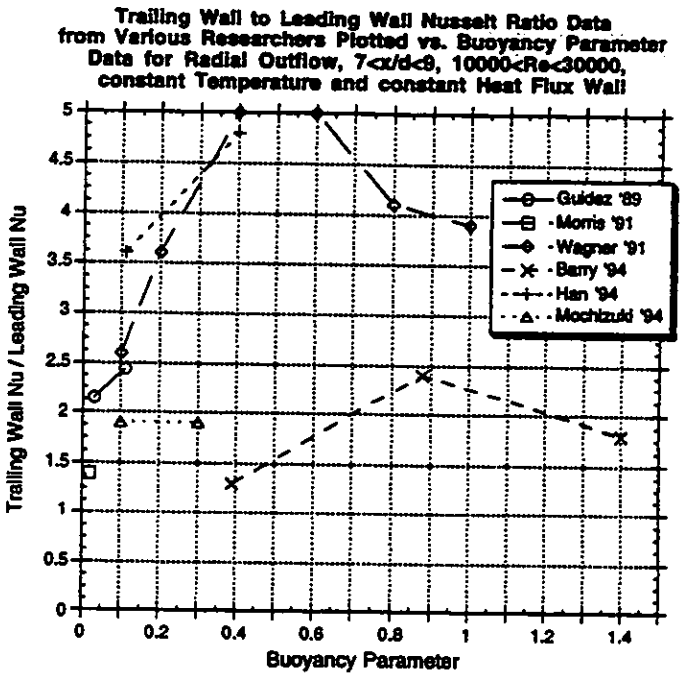

Figure 2: Rotating Heat Transfer Data from Various Researchers

subscripts
bulk - local mass averaged quantity
DB – Dittus-Boelter stationary Nusselt correlation (equation 3)
film - average of wall and bulk
in - passage inlet conditions
LS - leading passage wall
TS - trailing passage wall

INTRODUCTION

The hot section of a modern gas turbine engine operates with high inlet temperatures and aggressive blade loading to provide high specific power. These demands conflict directly with the limitations of engineering materials. To resolve this conflict bleed air from the compressor is used to cool turbine components. For the rotating turbine blade in particular cooling air flows through serpentine passages oriented along the span of the blade. Modern turbine design depends on reliable cooling schemes to achieve performance levels beyond the capabilities of blading materials alone. Because of its critical role, considerable effort has been expended to accurately predict the performance of turbine internal cooling. However, due to the rotating turbine frame of reference, standard pipe flow correlations for heat transfer are inadequate. Rotation introduces Coriolis and buoyancy accelerations which create secondary flow vortices and skew the mean flow profile. These flow non-uniformities result in non-homogeneous heat transfer from the different passage walls depending on their orientation (as depicted in Figure 1).

Flow in a heated rotating passage can be characterized by the Reynolds number, Re, the Rotation number, Rot, and the Buoyancy parameter, Bo, defined as:

$$Re = \frac{\rho d u_{in}}{\mu} \qquad Rot = \frac{\Omega d}{u_{in}} \qquad Bo = \frac{T - T_{in}}{T}\left(\frac{\Omega d}{u_{in}}\right)^2 \frac{R_m}{d} \qquad (1)$$

The effects of these parameters on the smooth-wall cooling passage Nusselt number have been the subject of numerous experimental and computational studies. Significant experimental work has been carried out by Morris (1981), Wagner et al. (1991), and Han et al. (1994) among others. These and other researchers have succeeded in mapping out many of the parametric trends in the performance of turbine cooling passages, specifically the trailing-to-leading wall Nu disparity. The differences between the various data sets are still large enough, however, to leave the designer without solid quantitative tools to account for the effects of rotation (Figure 2). This is because the underlying mechanisms causing these rotational effects on cooling are as yet relatively unexplored. The wall heat transfer is ultimately a product of the heated, rotating flowfield, which has only recently been measured in detail by Bons and Kerrebrock (1998). In their work, laser velocimetry measurements are made inside a rotating transparent passage which is simultaneously heated using thin film resistive heaters. This recent experimental data is the starting point for the CFD work reported here.

CFD has been used to calculate the flow in turbine cooling passages for over 20 years. Though initially laminar, most recent studies employ k-ε or more sophisticated Reynolds Stress or low Reynolds number models of turbulence. In an attempt to further refine these models several researchers (Howard et al., 1980, Tekriwal, 1994, and Bo et al., 1995, among others) have proposed modifications to the closure relations to account for Coriolis or buoyancy effects with varying degrees of success. To be sure, modeling results have provided valuable flow insights including the discovery of an additional vortex pair (making 4 vortices in all) at high Rot (Iacovides and Launder, 1991) and the prediction of flow reversal at high Rot on the leading wall (Prakash and Zerkle, 1992). However, all of the heated rotating computations use the flow

prediction to estimate Nu which is then compared with experimental data to assess code validity. A lack of detailed flow measurements in the heated, rotating frame has prevented direct comparison with velocity data and thus an adequate code validation. Accordingly, Dutta et al. (1994) leave a discussion of the effects of reverse flow unresolved because "without experimental data on flow characteristics no conclusion can be drawn at this stage". Similarly, Bo et al. (1995) preface their discussion of model results with the disclaimer, "No experimental data of the velocity field are yet available, but...".

The objective of this research is to provide the technical community with the first CFD code validation with comprehensive velocity and heat transfer measurements in a heated, rotating smooth-walled passage. The code is a commercially available product with several state of the art modeling options. Availability of velocity and Nu data for comparison permit conclusions to be drawn regarding model accuracy and allow critical fluid mechanisms to be identified. These are the specific contributions of this paper.

NUMERICAL MODEL

For all calculations in this study the commercial CFD code Fluent/UNS version 4.2 was used. The code solves the Reynolds-Averaged Navier-Stokes equations for the turbulent passage flow with additional terms for buoyancy and Coriolis accelerations in the momentum equation to account for rotation. The flow is steady in a reference frame attached to the rotating passage (Figure 1). To close the governing system of equations, the Fluent/UNS code has three modeling options: standard k-ε, ReNormalization Group (RNG) k-ε, and Reynolds Stress model (RSM). These are described at length in the Fluent manuals (1997) and only a brief summary is given here. The standard k-ε model uses the familiar turbulent viscosity formulation which is defined using two additional conservation equations for turbulent kinetic energy (k) and dissipation (ε). The RNG based k-ε model is derived from the instantaneous Navier-Stokes equations using a mathematical technique called Renormalization Group methods. It is more universally applicable than the standard k-ε model and is especially suited for swirling flows. The final model is RSM, which involves the calculation of the individual Reynolds stresses using differential transport relations outlined in the Fluent manual. Based on the recommendations of Howard et al. (1980) and Prakash and Zerkle (1992) for flow in low aspect ratio passages, no Coriolis or buoyancy terms were added to the closure models. Default constants for the various terms were employed in all cases. The turbulent Prandtl number was taken to be 0.85.

The systems of equations outlined above require special treatment in the presence of solid boundaries. The code has two approaches to modeling the near-wall region. One involves the use of wall functions, which rely on semi-empirical formulas to bridge the region between the wall and the fully-turbulent log region of the boundary layer. Standard and non-equilibrium wall functions are available with this approach, both of which are based on the work of Launder and Spalding (1974). The alternative approach involves the use of the one-equation model of Wolfstein (1969) in the viscosity affected near-wall region ($Re_y < 200$). Use of this alternative near-wall model is limited to the k-ε models in Fluent/UNS version 4.2, thus the Reynolds Stress model is only exercised using wall functions. The primary benefit of using the wall function approach vs. the near-wall model involves the efficient use of computational resources. Since the near-wall model resolves the viscous sublayer, the first cell center must be located at a $y^+ \approx 1$. For the wall functions on the other hand, the first cell should be located in the log region, thus $y^+ \approx 30$ (with a minimum of 12). This results in a requirement for more than 20 times the number of cells for the near-wall case than for the wall function cases. Accordingly, the near-wall model was run on a grid of 21x43x108 fluid cells (97524 total) in the half-passage domain vs. 6 x 13 x 58 cells (4524 total) for the wall function cases. The grid is composed of hexahedral cells in a non-uniform distribution with closer cell spacing on the trailing wall (due to the thinner boundary layer there). Grid refinement studies were conducted on both grids by increasing the cell count by approximately 50% while satisfying the first cell y^+ requirements. The results were within 2% for streamwise velocity and 5% for Nusselt number indicating that the selected grids are adequate.

The working fluid is air at a system pressure of approximately 4 atm. Molecular viscosity, μ, specific heat, c_p, and thermal conductivity, k, are all treated as functions of temperature. The laminar Prandtl number, Pr, is taken to be 0.71. Internal radiation was not considered. Nu is calculated using the difference between the local wall temperature and the fluid bulk temperature (the mass averaged fluid temperature at the corresponding x/d station).

The Fluent/UNS code uses a pressure-based finite volume formulation where all variables are stored at the cell center. To solve the equations of continuity and momentum, the pressure-velocity coupling algorithm SIMPLE was employed. For the cases with heat transfer, a staggered control volume storage technique (PRESTO) was used as well as an implicit body force treatment to speed up convergence in the presence of strong buoyancy forces. The iterative solution procedure was carried out by a line Gauss-Seidel elimination technique. A multigrid acceleration technique was used to decrease calculation times.

The constant heat flux boundary condition was applied on the external walls of the passage where the thin resistive film was located (Figure 3). Then the code solves Fourier's conduction equation in the solid wall. The model also incorporates the variation of the wall material's (quartz) thermal conductivity with temperature. Other external surfaces are treated as adiabatic. Unfortunately, velocity and turbulence data were not available at the passage inlet. Considering the short inlet used in the experimental facility (Figure 3), uniform velocity and temperature are applied at the inlet with a turbulence level of 1% and a lengthscale of 0.7mm. A zero normal gradient exit boundary condition is set at the passage exit (l=11.5cm).

EXPERIMENTAL DETAILS

The experimental facility used for this study is described in detail in Bons and Kerrebrock (1998) and only a brief overview is given here. The heated test section is mounted at the end of a 0.4m radius arm (R_i/d=40) which spins in an evacuated chamber. Cooling air at approximately 4 atm enters and exits the rotating arm and test section through seals located on the shaft. The test section (l/d=11.5) is manufactured from square-bore quartz tubing with a 10mm internal side dimension and 1.5mm thick walls (Figure 3). The test section draws from an inlet plenum with an area ratio of 10. The center

90mm along each of the four exterior walls is coated with a 10mm wide swath of Indium Tin Oxide (ITO) which allows resistive heating of the passage. The thin film of ITO and the quartz substrate provide 80% transmission at the visible wavelength of the laser used for optical velocity measurement. Seed particles added to the airflow allow the use of the Particle Image Velocimetry (PIV) technique for acquiring 2-component velocity fields at various locations in the passage. Velocity measurements have a 6% uncertainty in the center 8mm of the passage. This uncertainty rises to 15% near the walls due to increased optical noise. Passage exterior wall temperatures are measured using an infrared scanning temperature measurement system. From this measurement of wall temperature and the known constant heat flux generated in the ITO the internal wall Nu is calculated with an absolute uncertainty of 9%.

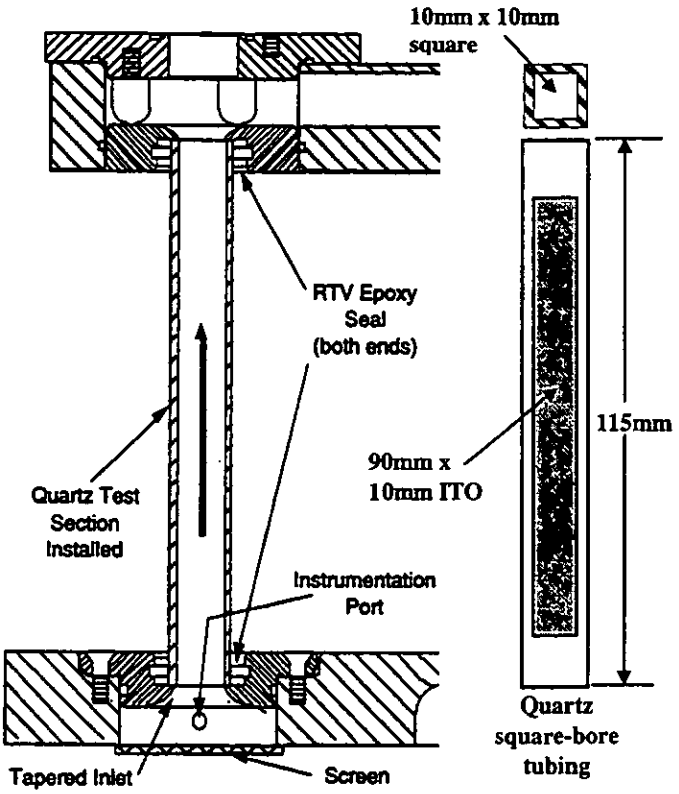

Figure 3: Schematic of Experimental Test Section

RESULTS AND DISCUSSION

The results are presented in increasing levels of complexity, beginning first with the stationary isothermal case and evolving finally to the rotating, heated passage flow with wall conduction. In each case the calculations are compared to the experimental data from Bons (1997). Bons' flow velocity data was extracted from PIV images which were reduced into 2-component vector fields. The orientation of the PIV light sheet allowed access to a plane normal to the axis of rotation (x-z plane, see Figure 1). Since the strongest velocity gradients were expected in the y and z (non-radial) directions the vector field from each PIV image was first averaged along the x direction (yielding u(z) and w(z) for each image). Due to observed randomness in the vectors, four to six images were combined to produce ensemble-averaged u(z) and w(z) distributions at a given x and y position. The light sheet and camera were then translated in the y and x direction to obtain ensemble averaged u(z) and w(z) distributions at various positions in the passage. u(z) and w(z) at the same x but various y positions were then "stacked-up" to provide a quasi-3D look at the flowfield (assuming the mean flow is steady). Then u(y) and w(y) distributions were generated at this same x location by interpolating between images in the y direction.

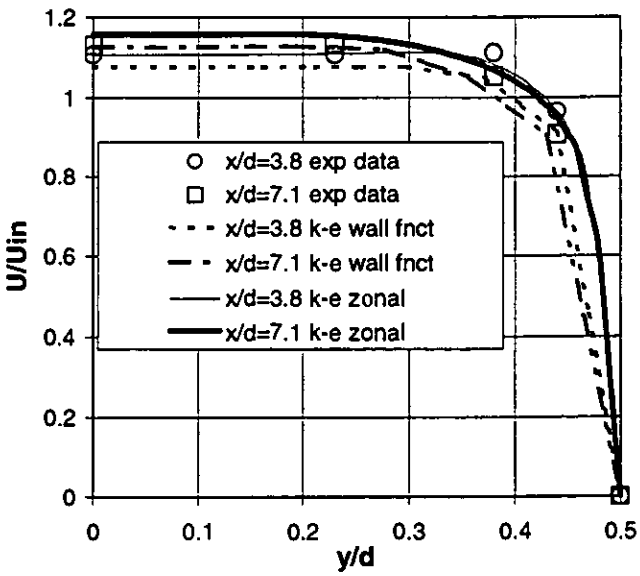

Figure 4: Rot=0, Re=10000, Bo=0. Streamwise Velocity Profiles for Data vs. k-e with Wall Function and Zonal Model (z/d = 0.5)

Stationary Isothermal Passage Flow

Figure 4 shows u(y) data for Re=10000 and Rot=0 at two x/d locations. Also shown are model predictions using the standard k-ε model with both standard wall functions and the 2-layer zonal model. Though the experimental data were only taken at 4 y/d planes, the 2-layer zonal model appears to give a bener fit to the data at both x/d stations. Both the features of boundary layer development and passage core acceleration are adequately captured. This figure justifies the choice of velocity and turbulence inlet conditions.

Rotating Isothermal Passage Flow

The effect of rotation on the passage flow is shown in Figures 5a&b for the k-ε with 2-layer zonal model at x/d=7.9. The u contour plot in Fig 5a shows the streamwise velocity profile skewed to the trailing wall and Fig 5b shows the passage double vortex located favoring the leading wall of the passage (only half the passage is shown due to symmetry). A comparison with the experimental data is made in Figures 6a&b at x/d=7.9 for Re=8000 and Rot=0.2. Figure 6a also includes the w(y) calculations obtained with all 3 models exercised using standard wall functions. All of the models dramatically underpredict the vortex extent and strength, even with the estimated experimental uncertainty of 15% (Bons, 1997) in the velocity vectors near the side wall. The zonal model is the most

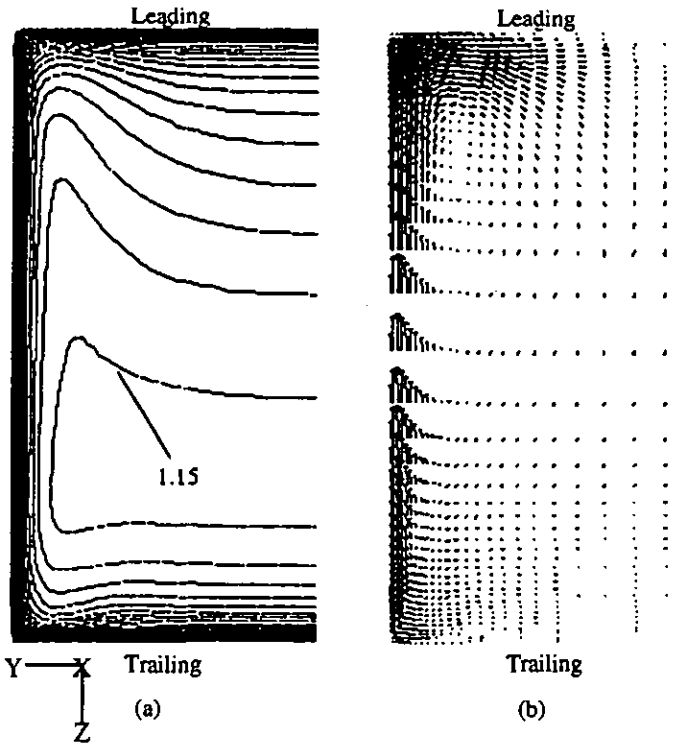

Figure 5: Rot = 0.2, Re = 8000, & Bo = 0. k-ε Zonal Model Prediction at x/d=7.9. (a) u/u_a Contour Plots, 0.05/division (b) In-plane Vector Field.

accurate with a peak velocity in the vortex of only half the measured value (vs. one fifth for the others) and a zero velocity crossing point (vortex center) of y/d=0.1 from the wall (vs. 0.15 for the other models). The Coriolis vortex has its origin in the boundary layer velocity defect on the side walls. Since the zonal model has over eight times as many nodes in this region than the standard wall function (with a first node $y^+>12$), it properly accounts for the secondary flow growth and limits its diffusion from the wall. Choi et al. (1989) found wall functions to be similarly unsuitable for three-dimensional turbulent internal flow in a non-rotating curved duct. Small pressure variations across the sublayer (especially near the passage corners) play a significant role in shaping the secondary motion in the passage, which is ultimately a key factor in predicting the primary flowfield. Since the use of wall functions completely overlooks variations below the log layer, it is incapable of adequately accounting for these effects.

The fact that none of the models predict the appropriate size of the Coriolis vortex indicates that they may be overly dissipative in the boundary layer. This is supported by a look at the vortex development with x/d (Figure 7). The vortex appears to reach a maximum at x/d=4 while the recently published experimental data [Tse and McGrath (1995), Servouse (1998), and Bons and Kerrebrock (1998)] indicate continued vortex growth up to x/d=10.

Figure 6b shows the u(z) comparisons from the same suite of models along with the experimental data. Here all the models have an 8-10% larger core acceleration (in the region 0.3<z/d<0.9) than the experimental data. A visual comparison of the various models and

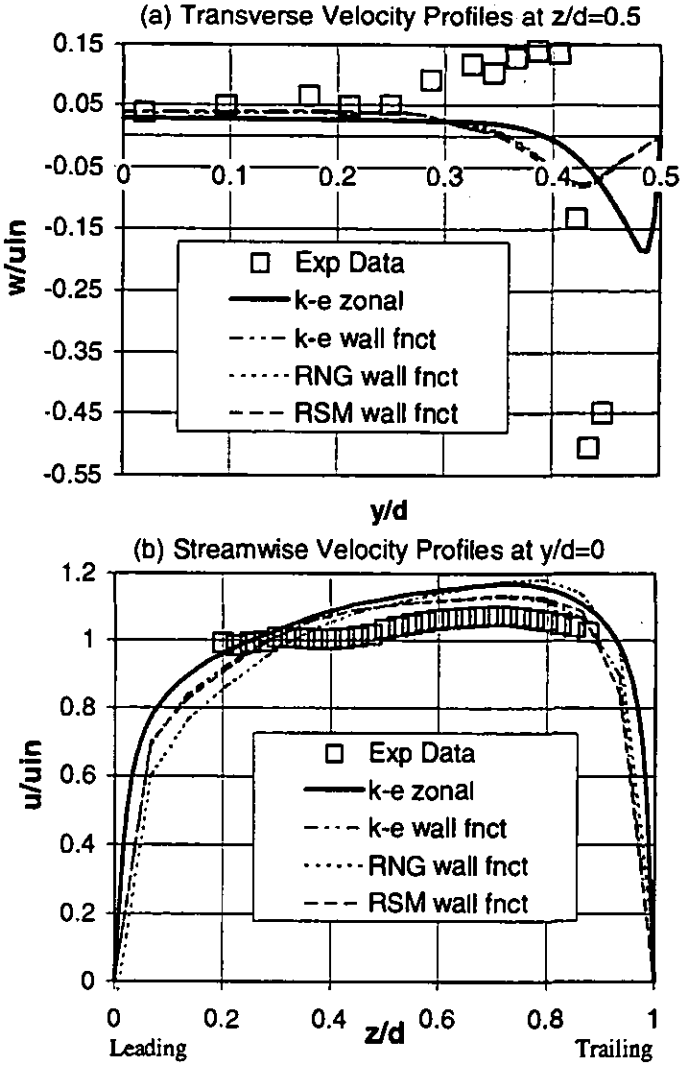

Figure 6: Rot = 0.2, Re = 8000, & Bo = 0. Data vs. 4 Models
(a) w(y) Transverse Velocity Profiles at z/d = 0.5
(b) u(z) Streamwise Velocity Profiles at y/d = 0.

data in this region shows that the shape (though not the mean value) of the k-ε zonal model calculation is closer to the data than the others. The RNG model has a steeper slope, and the RSM and standard k-ε models (with wall functions) aren't as flat near the leading wall as the zonal model and data. The fact that the mean u of the models are all higher than the data can be understood by referring to intuition gained from the momentum integral model results presented in Bons and Kerrebrock (1998). There are two Coriolis acceleration components in the governing momentum equation. The $+2\Omega u$ component in the z-momentum equation creates the Coriolis vortex. Once this secondary flow is established, the $-2\Omega w$ component in the x-momentum equation causes an acceleration of the near side-wall fluid in the streamwise direction and depresses the passage core velocity. Since it is proportional to w, this second component is quite weak until the vortex strength rises to an appreciable level. Because the

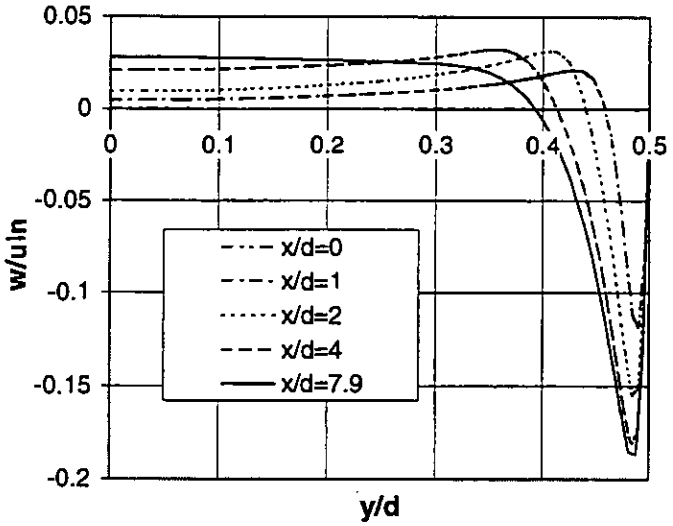

Figure 7: Rot = 0.2, Re = 8000, & Bo = 0. Transverse w(y) Velocity Profiles at 5 x/d for k-ε Zonal Model (z/d = 0.5).

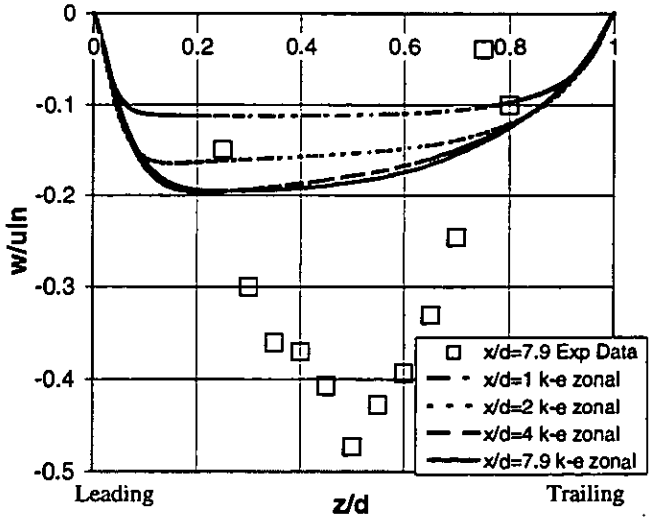

Figure 9: Rot = 0.2, Re = 8000, & Bo = 0. Transverse w(z) Velocity Profiles in the Near Side-Wall Region (y/d = 0.485) for Data (at x/d = 7.9)vs. k-ε Zonal Model (at 4 x/d).

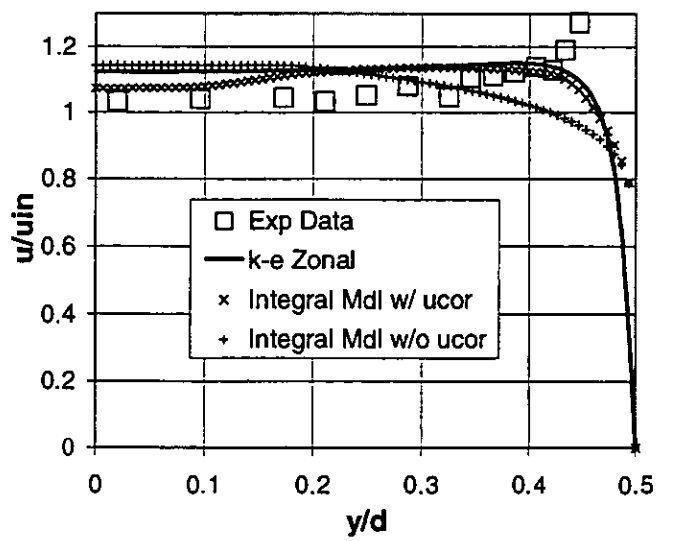

Figure 8: Rot = 0.2, Re = 8000, & Bo = 0. Sreamwise u(y) Velocity Profiles for Data vs. k-ε Zonal Model vs. Integral Model Results (with and without 2nd Coriolis component). x/d = 7.9 & z/d = 0.5.

experimental vortex strength is nearly twice that of the nearest model the effect of this second component is also underpredicted by the models. Figure 8 shows u(y) for the k-ε zonal model and the experimental data along with the momentum integral model results calculated with and without the 2nd Coriolis component (denoted ucor in the plot). Note the slight rise in the zonal model prediction of u as the wall is approached. If the vortex strength were doubled to match the data, this rise would increase and depress the core streamwise velocity to more nearly match the data (as it does with the momentum integral model).

Others have experienced similar difficulties in matching rotating passage flow features. Berg et al. (1991) compared a k-ε model calculation with LDA data taken in a circular tube at Re=40000 and Rot=0.04. The model overpredicted the maximum u velocity by 17% with a greatly exaggerated slope from leading to trailing wall. Younis (1993) also shows an exaggerated u(z) skew in his model comparison with Wagner and Velkoff's (1972) early hot wire data. Interestingly, Younis employs a k-ε model with a non-linear stress strain relation and one of Howard et al.'s (1980) Coriolis modifications. Howard et al. realized much better agreement with the same Wagner and Velkoff flow data by employing no modifications to the standard k-ε formulation. This was then the basis for their recommendation against the use of Coriolis modifications for low aspect ratio (square) passages.

None of the models presented herein show signs of a second vortex pair forming near the trailing wall of the passage. To the author's knowledge, no one has yet experimentally verified the presence of this second vortex pair though a number of model calculations presented in the literature predict its existence. The data from Bons (1997) show no evidence of the second vortex pair, though data very near the passage walls is sparse due to optical limitations. Those researchers who have predicted its existence have shown it's presence to be sensitive to Re (Iacovides and Launder, 1991), initial conditions (Prakash and Zerkle, 1992), modeling of dissipation (Dutta et al., 1994), passage aspect ratio (Younis, 1993), and x/d (Bo et al., 1995). Thus the conditions in the passage under current evaluation may not be suitable for the formation of the second vortex pair. Indeed Prakash and Zerkle openly assert from their findings that "the four vortex solution may not occur in short ducts where the flow is not fully developed".

As noted previously in Figure 5b, the model prediction puts the Coriolis vortex closer to the leading wall than the trailing wall. Looking at w(z) profiles (Figure 9) at y/d=.485 (at the vortex maxima

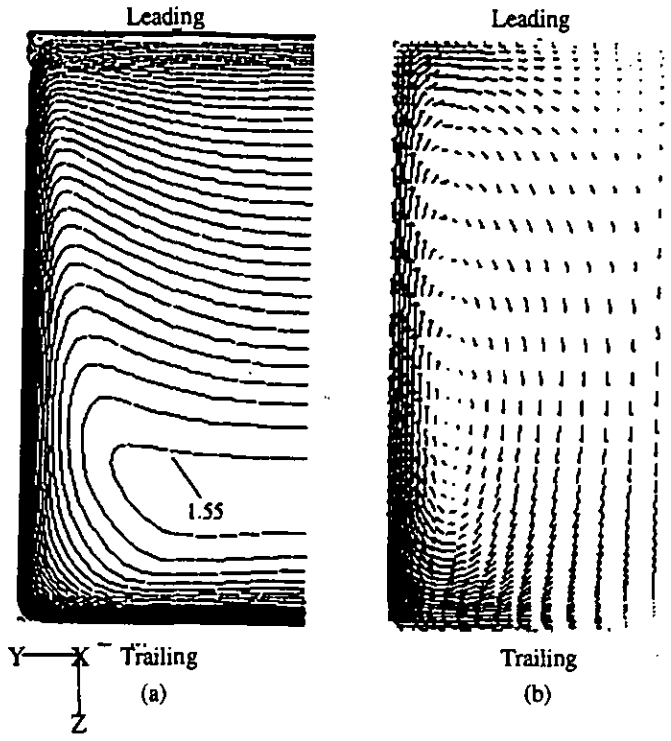

Figure 10: Rot = 0.2, Re = 8000, & Bo = 0.49. k-ε Zonal Model Prediction at x/d=7.9. (a) u/u_{in} Contour Plots, 0.05/division (b) In-plane Vector Field.

near the side wall) the vortex peak velocity migrates to the leading wall with x/d. This figure also includes the experimental data from the same case (data at x/d=7.9 only). As noted earlier, the magnitude is significantly larger for the data, but note also that the experimentally measured vortex appears centered on the passage side wall. This may also explain the stunted growth of the vortex as predicted by the model compared with the continued growth with x/d documented in the data. With the vortex lateral migration, its growth may be more constrained by the presence of the leading wall than if it had remained centered on the side wall.

Heated, Rotating Velocity Measurements

With the addition of heat and the associated buoyancy forces, the rotating passage flow is altered considerably. Again the contour map of u and in-plane vectors at x/d=7.9 are shown for the k-ε with 2-layer zonal model (Figures 10a & b). In this case, a constant heat flux value of 10 kW/m^2 (the mean of the 4 walls in the experiment) is applied as the boundary condition at the exterior passage walls. The code is then run in the conjugate heat transfer mode, solving both the conduction in the solid walls and the turbulent flow in the passage simultaneously to determine the fluid/solid wall interface temperature and heat flux. The result is a buoyancy parameter value of 0.49 (density ratio=0.27) with Rot=0.2 and Re=8000.

As noted by others (Prakash and Zerkle, 1992), the vortex has moved to the trailing wall with the increase in density ratio (from 0 to 0.27), as has the bulk of the core flow. A narrow region of reverse

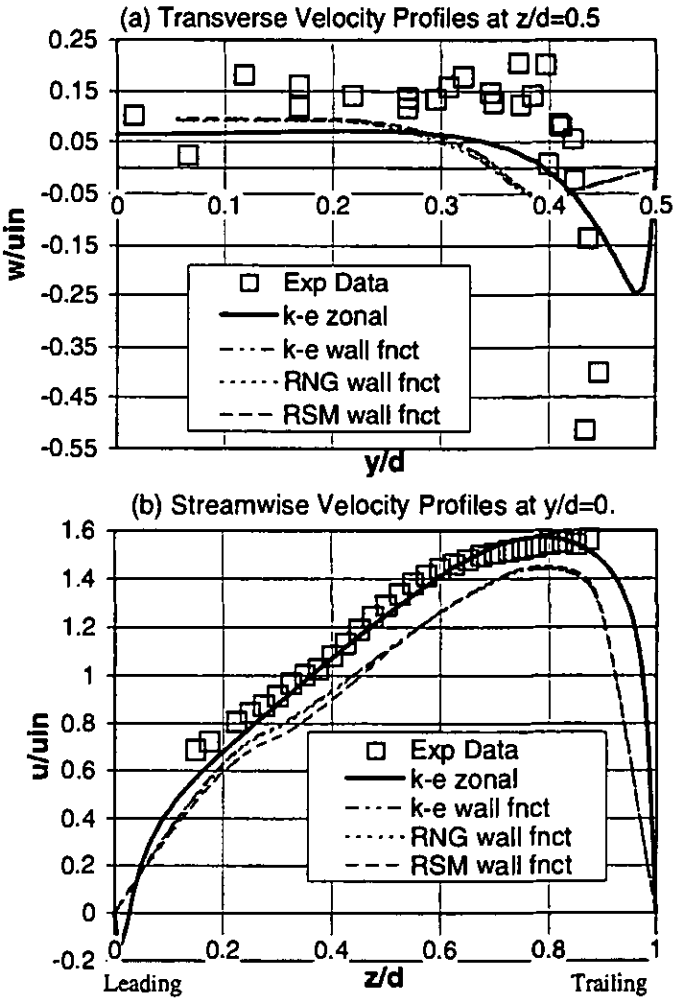

Figure 11: Rot = 0.2, Re = 8000, & Bo = 0.49. Data vs. 4 Models (a) w(y) Transverse Velocity Profiles at z/d = 0.5 (b) u(z) Streamwise Velocity Profiles at y/d = 0.

flow is located near the leading wall (z/d<0.05) of Figure 10a (also Figure 14). Note the remarkable agreement between the zonal model calculation and the experimental u(z) profile in Figure 11b. As presented in Bons and Kerrebrock (1998), several of the PIV vector images manifest intermittently stagnant flow near the leading wall at x/d=7.9, which is consistent with the prediction of the model as seen here. Prakash and Zerkle (1992) and Tekriwal (1994) both predicted strong reverse flows in modeling the Wagner et al. (1989) experimental data set. Dutta et al. (1994) however did not calculate reverse flow for the identical case, a fact which was attributed to the use of a Coriolis-modified k-ε model. The disagreement can perhaps be better explained by the disparate boundary conditions employed by the various models. Prakash and Zerkle and Tekriwal used a fully developed inlet velocity field (modeling a long unheated starting length duct) while Dutta et al. used a flat inlet velocity profile. Also, Dutta specified no reverse flow at the exit plane, while the others used the no-gradient exit condition. The present model employs a flat inlet

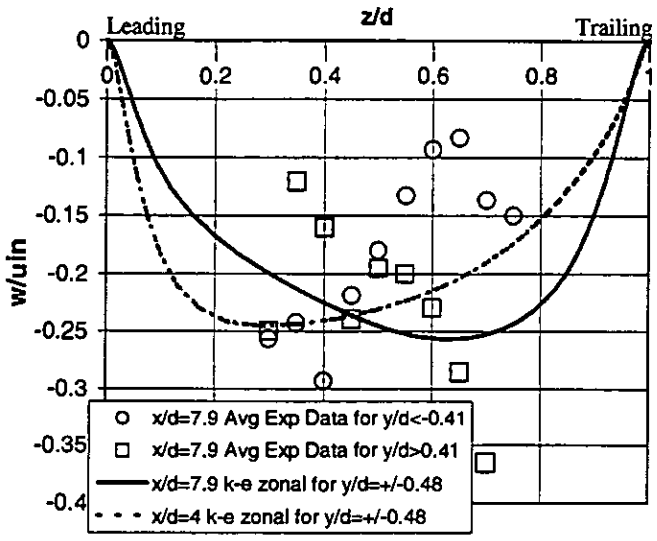

Figure 12: Rot = 0.2, Re = 8000, & Bo = 0.49. Transverse w(z) Velocity Profiles in the Near Side-Wall Region. Data (at y/d > 0.41 & y/d < -0.41 with x/d = 7.9) vs. k-ε Zonal Model (at y/d = 0.48 for 2 x/d).

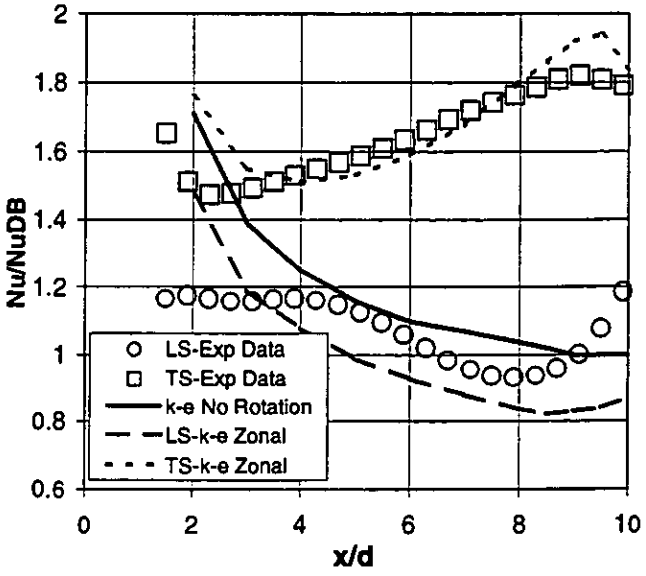

Figure 13: Rot = 0.2, Re = 8000, & Bo = 0.49. Wall Laterally-Averaged Nusselt Number Ratio vs. x/d. Data vs. k-ε Zonal Model for Trailing and Leading Walls. (Rot = 0 case shown for reference)

velocity profile to match the experimental configuration. This and the proper exit condition (no constraint on reverse flow) create an excellent agreement between the model and the experimental u(z) profile. This underscores the importance of faithfully reproducing the experimental inlet conditions for accurate flow calculations.

Also in his study, Tekriwal (1994) found that the level of a critical non-dimensional parameter ($Gr_\Omega/Re^2 = Ra_\Omega/ Pr\ Re^2$) determined the presence of reverse flow in his several predictions. This parameter (referred to as the buoyancy parameter, Bo, here) is defined as:

$$Bo = \frac{\beta(T - T_{in})\Omega^2 R_m d^3}{\nu\alpha}\left(\frac{\alpha}{\nu}\right)\left(\frac{\nu}{ud}\right)^2 = \frac{Ra_\Omega}{Pr\,Re^2} \qquad (2)$$

Tekriwal found the cut-off point for the Wagner et al. (1989) configuration to be somewhere between Bo = 0.25 and 0.37. For the highest buoyancy number case (Bo = 1.47) of Wagner et al., Tekriwal predicts a reverse flow of u/u_{in} = -0.2 at x/d=8. Prakash and Zerkle predict a much higher reverse flow of over u/u_{in} = -0.5 at x/d=10 for the same Bo case. Because of the differences between the Bons (1997) and Wagner et al. experimental configurations (different inlet conditions and wall heating method), it is not evident that the same threshold level of Bo would apply in both cases. Nevertheless, the current case has a Bo=0.49, well above the Tekriwal-defined threshold and the calculation indicates a maximum reverse flow at x/d=7.9 of u/u_{in} = -0.22. While the magnitude of the reverse flow does not compare well between the three simulations, the location of the reverse flow region is identical in all three cases, that being near the corners of the leading wall. The hot boundary layer wall fluid is constantly fed to these corners by the action of the Coriolis vortex and it is thus most adversely affected by centrifugal buoyancy (Figure 10a).

In contrast with the excellent agreement of the u(z) profile, the Coriolis vortex strength prediction is still lacking. The peak velocity is again only half of the measured value (as shown in Figure 11a). As in the non-heated case, the model attenuates the Coriolis effect in the sidewall boundary layer much more than shown by the data. The fact that the u(z) is so well captured while w(y) is still lacking indicates that the model adequately accounts for the buoyancy terms in the core flow region but falls short with the Coriolis terms near the walls. Perhaps this points to the need for some Coriolis modeling in the k-ε closure equations as recommended by several researchers (Khodak et al., 1993, Dutta et al., 1994, and recently Saidi and Sunden, 1998), though this runs counter to Howard et al.'s (1980) conclusion for low aspect ratio passages cited earlier.

The standard wall function model results (also indicated in Figures 11a & b) show reasonable agreement in u(z) but are again lacking in the prediction of w(y). As mentioned above, the buoyancy which creates the u(z) skew is a bulk flow effect, while the Coriolis forces which generate the vortex are confined to a narrow region near the wall. Thus the wall function approach is adequate for predicting the bulk flow but not for the secondary flow. A third wall function option available in the Fluent code, the non-equilibrium wall funcuons, was also exercised with the 3 different closure models but produced a spectactularly bogus result. The passage Coriolis vortex is produced, but with the opposite (incorrect) sign. Though based on the formulation developed by Launder and Spalding (1974), which was employed successfully by Dutta et al. (1994), the incorporation here is evidently not well suited for this flowfield. This same non-physical result is produced when the non-equilibrium wall functions are used in the isothermal flow case.

Comparing Figures 5b and 10b it is obvious that the increase in density ratio (from 0 to 0.27) causes a shift of the vortex position from the leading to the trailing wall. This was also shown in the Prakash

and Zerkle (1992) calculation as the density ratio was increased from 0.01 to 0.13. Since the axial velocity is significantly higher at the trailing wall (due to the skew caused by buoyancy), the u(y) side-wall boundary layer gradients responsible for the vortex formation are correspondingly stronger. Thus the vortex strength migrates from the leading wall at the inlet to the trailing wall at x/d=7.9 along with the majority of the core flow (Figure 12). This migration brings the vortex in closer proximity to the trailing wall and increases the measured heat transfer there as will be discussed later. The experimental data is inconclusive in this regard, with vectors on one side wall showing the vortex closer to the trailing wall while the vortex is nearer to the leading wall on the opposite side (also in Figure 12). This brings up one experimental feature not captured by the model. The model assumes a steady mean flowfield in the passage, employing as it does the Reynolds-Averaged Navier-Stokes equations. The experimental flowfield was imaged using PIV which gives an instantaneous image of the 2D velocity field. Each data point in Figure 12 represents the ensemble-average of 4-6 consecutive PIV vector fields, thus approaching the steady mean flow assumption of the model. There is nothing to suggest, however, that the vortex position is in reality steady in space. While the u(z) experimental data did appear entirely consistent through all the PIV images, the variations in w were considerable and suggest a vortex that may dilate or expand and perhaps translate from leading to trailing wall in the passage. These variations in the experimental vortex measurements for the heated case were not reproduced in the isothermal data, suggesting that the instability creating the variations may be related to buoyancy. Lateral (y-direction) vortex motion is not supported by the PIV data, the w>0 central portion of the passage remaining virtually constant throughout the data set.

Heat Transfer Measurements

Unlike the internal flowfield, wall heat transfer in a rotating cooling passage has been documented by numerous researchers over the years. Figure 13 shows the k-ε zonal model predictions for the leading and trailing wall Nu with the corresponding data. The plots of laterally-averaged Nu(x) shown here are normalized by the Dittus-Boelter (1930) correlation for Nu in a stationary tube.

$$Nu_{DB} = 0.023\,Pr^{0.4}\,Re^{0.8} \qquad (3)$$

The Nu prediction for the stationary passage is added to Figure 13 to demonstrate the fidelity of the model in the baseline case. Both the leading wall droop and the trailing wall rise in Nu are slightly more accentuated in the model than in the data, but the trends are well matched. In the region $2.5 < x/d < 8.5$ the model is within the experimental uncertainty of the data. Outside this region, the trailing wall agreement is fair while the leading wall agreement worsens considerably (perhaps due to passage end effects not modeled properly in the code). On the trailing wall, the rise in Nu which begins at x/d=5 corresponds well to the first indication of predicted reverse flow on the leading wall (see Figure 14). The near-wall fluid stagnates on the leading wall creating a significant blockage in the passage which accelerates the motion of cold core fluid to the trailing wall. This

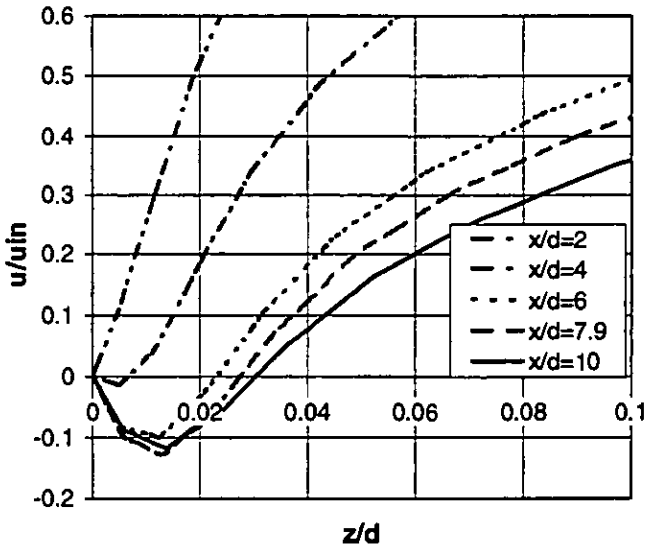

Figure 14: Rot = 0.2, Re = 8000, & Bo = 0.49. Closeup of Streamwise u(z) Velocity Profiles at various x/d & y/d = 0. k-ε Zonal Model Predictions. (Note region of reverse flow)

enhances the Nu on the trailing wall at the same time creating an effective barrier to convection on the leading wall.

The trailing-to-leading Nu ratios for the data and 4 computational cases are plotted in Figure 15. As noted before, the zonal model provides a good match early in the passage but overpredicts this ratio beyond x/d=8. The other models match the experimental Nu value at x/d=8, but fall short of the data upstream and overpredict the ratio further downstream. The wall function models' actual Nu predictions (not the Nu_{TS}/Nu_{LS} ratio shown here) are 10 to 20% lower than the zonal model predictions for both the leading and trailing wall (thus they are even further from the experimental data in the absolute sense). The role of the different near-wall turbulence models in creating these disparities can perhaps be more clearly understood by examining the predicted turbulence field, as did Bo et al. (1995). Figures 16a & b show the development of turbulence intensity with x/d along the centerline plane using the k-ε model with two different wall treatments: (a) 2-layer zonal model and (b) standard wall functions. Though both cases show the gradual rise with x/d, the levels are much higher with the zonal model. In addition, the distribution across the centerline is much more non-uniform in the zonal model and bears a striking resemblance to the profiles produced by Bo et al.'s low Re ASM model. Bo et al. attributed this effect to the second moment closure of the ASM model, while here it is evidently a product only of the wall treatment and the associated grid refinement. Whether this difference is solely responsible for the better agreement of the zonal model's Nu and flow prediction with the data is uncertain. It is clear though that the finer wall treatment produces a markedly different turbulence profile throughout the passage and not just in the sublayer.

As a final note, the experimental configuration in Bons (1997) was not one of identical heat flux from 4 passage walls as has been modeled here. Due to a manufacturing error, one side wall generated nearly 20% more heat while the other generated 12% less heat than the

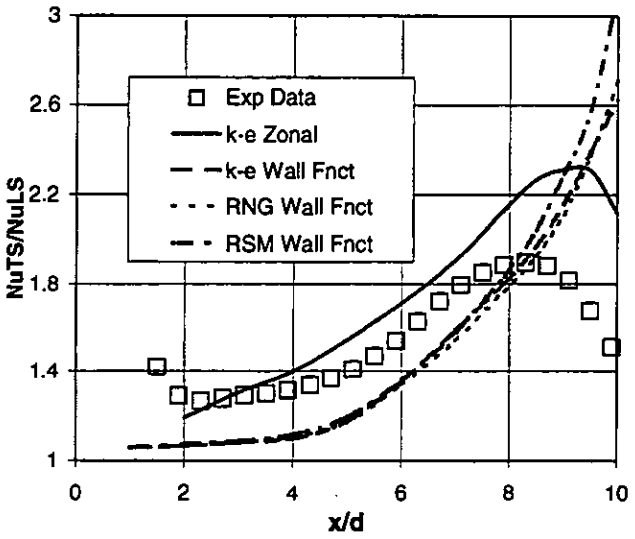

Figure 15: Rot = 0.2, Re = 8000, & Bo = 0.49. Wall Laterally-Averaged Trailing-to-Leading Wall Nusselt Ratio vs. x/d. Data vs. k-ε Zonal Model and 3 Models with Wall Functions.

leading and trailing walls (which were well matched at approximately 10kW/m^2). To model this imbalance accurately using the k-ε zonal model would require double the number of computational cells since passage symmetry is negated. Since this is computationally prohibitive at the present time, the zonal model was only run on a half passage with the identical heat flux from each wall. To provide some assessment of the effect of this imbalance, the standard wall function case was run on the full passage with the accurate heat flux distribution. The laterally-averaged Nu values on the leading and trailing walls were relatively unchanged from the symmetric case though the spatial distribution was skewed somewhat to the corners. The bulk flowfield was also relatively unchanged for the full passage case. The hotter side wall showed a slightly higher Nu than the "cold" side wall (about 5%), though not nearly as exaggerated as in the experimental data (Bons, 1997). Given the shortcomings of the wall function model exposed above, a final determination will have to await the use of the zonal model on the full passage calculation. Since the conclusions made in this paper are drawn from the flowfield and the laterally-averaged Nu data on the leading and trailing wall only (which are virtually unchanged with the full passage calculation), this imbalance should not invalidate the findings documented herein.

CONCLUSIONS

A commercially available CFD code was used to calculate the flowfield and heat transfer in a simulated turbine cooling passage (with smooth walls). Direct comparisons are made with wall heat transfer and flow velocity data available from Bons (1997). The test section was operated with radial outward flow and at values of Reynolds number, rotation number, and buoyancy parameter typical of applications. The conclusions of the study are as follows:

1) The most important conclusion regards the use of wall treatments in k-ε type turbulent flow calculations. Both the flow

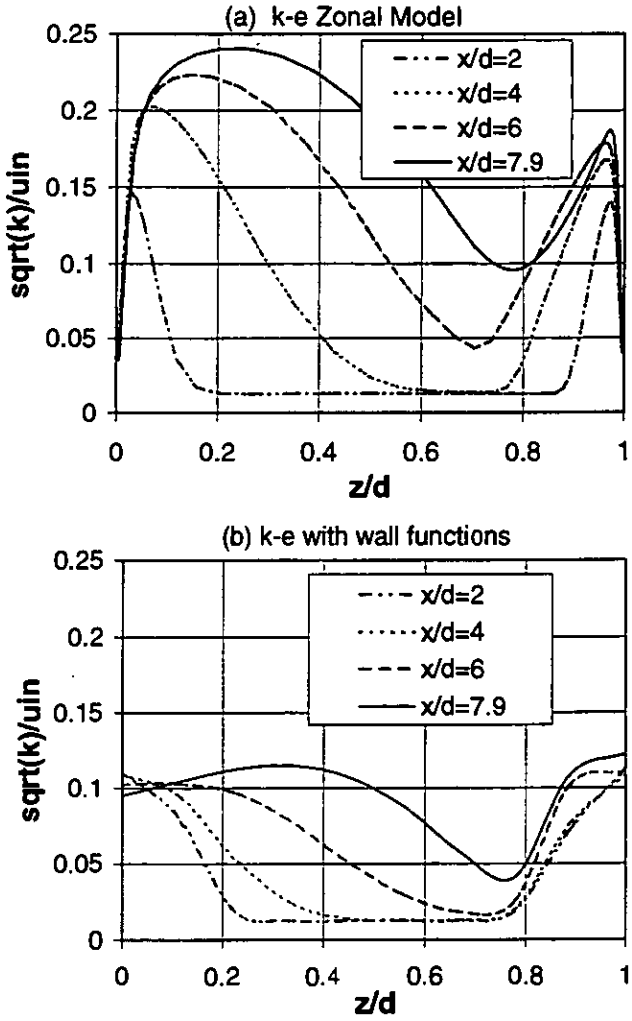

Figure 16: Rot = 0.2, Re = 8000, & Bo = 0.49. Turbulence Intensity Profiles at y/d = 0 and various x/d. (a) k-ε Zonal Model (b) k-ε Model with Wall Functions

and wall Nu comparisons bear out that wall functions are inadequate for this complex flowfield. They consistently underpredict the secondary flow and provide a poor estimate of the passage heat transfer compared to the near-wall zonal model. The gain in accuracy with the zonal model comes at a significant penalty in computation time, however, as the number of fluid (and solid) cells increases by more than 20 times.

2) A comparison of 3 different closure models (standard k-ε , RNG k-ε , and RSM all with wall functions) shows significantly less variation than from the wall treatment. Though not presented, the RNG model, when coupled with the finer 2-layer zonal wall treatment produces results comparable to those presented for the standard k-ε model. It is not possible to operate the RSM model with the 2-layer zonal model in FLUENT/UNS v4.2, though this is a capability available in the next release and may provide some improvement.

3) As for the accuracy of the flowfield calculation, the model appears to capture the effect of buoyancy on the core flow quite well.

The agreement between the calculated and measured streamwise velocity profile, u(z), is remarkable. This contributes to a reasonably good leading and trailing Nu match with the data. This agreement is obtained without any buoyancy terms in the k or ε conservation equations. The comparison of the predicted Coriolis vortex strength with the data is not as good. The calculated maximum vortex velocity only reaches half that of the measured vortex. The calculated vortex position and development with x/d are also not entirely in line with the experimental data.

4) Finally, to the author's knowledge, this represents the first CFD validation for this complex industrial flowfield which includes both a comparison of wall heat transfer and flow velocities. The simultaneous evaluation of both of these features is shown to be critical to understanding the code's limitations.

ACKNOWLEDGEMENTS

This work was performed under partial sponsorship from the Air Force Office of Scientific Research, with Dr. Mark Glauser as contract monitor.

REFERENCES

Barry, P., 1994, "Rotational Effects on Turbine Blade Cooling", Master's Thesis, Department of Aeronautics and Astronautics, Massachusetts Institute of Technology, Cambridge, MA.

Berg, H., Hennecke, D., Elfert, M., and Hein, O., 1991, "The Effect of Rotation on Local Coolant Side Flow and Heat Transfer in Turbine Blades", ISABE 91-7016, published by AIAA, pp. 170-183.

Bo, T., Iacovides, H., and Launder, B.E., 1995, "Developing Buoyancy-Modified Turbulent Flow in Ducts Rotating in Orthogonal Mode", ASME Journal of Turbomachinery, Vol 117, pp. 474-485.

Bons, J., 1997, "Complementary Velocity and Heat Transfer Measurements in a Rotating Turbine Cooling Passage", PhD Thesis, Department of Aeronautics and Astronautics, Massachusetts Institute of Technology, Cambridge, MA.

Bons, J.P., Kerrebrock, J.L., 1998, "Complementary Velocity and Heat Transfer Measurements in a Rotating Cooling Passage with Smooth Walls", presented at the ASME IGTI 98 in Stockholm, Sweden, June 2-5, 1998, ASME paper number 98-GT-464.

Choi, Y.D., Iacovides, H., and Launder, B.E., 1989, "Numerical Computation of Turbulent Flow in a Square-Sectioned 180° Bend", ASME Journal of Fluids Engineering, Vol. 111, pp. 59-68.

Dittus, F.W., and Boelter, L.M.K., 1930, University of California Publications, Vol 2, pg. 443.

Dutta, S., Andrews, M., and Han, J.C., 1994, "Numerical Prediction of Turbulent Heat Transfer in a Rotating Square Duct with Variable Rotational Buoyancy Effects", presented at the 6th AIAA/ASME Thermophysics and Heat Transfer Conference, Colorado Springs, CO, June 20-23.

Fluent/UNS and Rampant User's Guide, 1997, version 4.2, Vol I-IV, Fluent Inc.

Guidez, J., 1989, "Study of the Convective Heat Transfer in a Rotating Coolant Channel", ASME Journal of Turbomachinery, Vol. 111, pp. 43-50.

Han, J., Zhang, Y., and Lee, C., 1994, "Influence of Surface Heating Condition on Local Heat Transfer in a Rotating Square Channel with Smooth Walls and Radial Outward Flow", ASME Journal of Turbomachinery, Vol. 116, pp. 149-158.

Howard, J.H.G., Patankar, S.V., and Bordynuik, R.M., 1980, "Flow Prediction in Rotating Ducts Using Coriolis-Modified Turbulence Models", ASME Journal of Fluids Engineering, Vol. 102, pp. 456-461.

Iacovides, H. and Launder, B., 1991, "Parametric and Numerical Study of Fully Developed Flow and Heat Transfer in Rotating Rectangular Ducts", ASME Journal of Turbomachinery, Vol. 113, pp. 331-338.

Khodak, A., Kirillov, A., Ris, V., and Smirnov, E., 1993, "Local Heat Transfer in 3-D Turbulent Flow through Ducts Rotating in the Orthogonal Mode", 8-IC-14, pp. 261-266.

Launder, B.E. and Spalding, D.B., 1974,"The Numerical Computation of Turbulent Flows", *Computer Methods in Applied Mechanics and Engineering*, Vol. 3, pp. 269-289.

Mochizuki, S., Takamura, J., Yamawaki, S., and Yang, Wen-Jei, 1994, "Heat Transfer in Serpentine Flow Passages with Rotation", ASME Journal of Turbomachinery, Vol. 116, pp. 133-140.

Morris, W., 1981, *Heat Transfer and Fluid Flow in Rotating Coolant Channels*, Research Studies Press.

Morris, W. and Ghavami-Nasr, G., 1991, "Heat Transfer Measurements in Rectangular Channels with Orthogonal Mode Rotation", ASME Journal of Turbomachinery, Vol. 113, pp. 339-345

Prakash, C. and Zerkle, R., 1992, "Prediction of Turbulent Flow and Heat Transfer in a Radially Rotating Square Duct", ASME Journal of Turbomachinery, Vol. 114, pp. 835-846.

Saidi, A. and Sunden, B., 1998, "Calculation of Convective Heat Transfer in Square-Sectioned Gas Turbine Blade Cooling", presented at ASME IGTI 98 in Stockholm, Sweden, June 2-5, 1998, ASME paper #98-GT-204.

Servouse, T., 1998, "3D Laser Anemometry in a Rotating Cooling Channel", presented at ASME IGTI 98 in Stockholm, Sweden, June 2-5, 1998, ASME paper #98-GT-123.

Tekriwal, P., 1994, " Heat Transfer Predictions with Extended k-ε Turbulence Model in Radial Cooling Ducts Rotating in Orthogonal Mode", ASME Journal of Heat Transfer, Vol. 116, pp. 369-380.

Tse, D. and McGrath, D., 1995, "A Combined Experimental/Computational Study of Flow in Turbine Blade Passage: Part I - Experimental Study", ASME Paper #95-GT-355, presented at ASME IGTI, Houston, Texas, June.

Wagner, J., Johnson, B., and Hajek, T., 1991, "Heat Transfer in Rotating Passages with Smooth Walls and Radial Outward Flow", ASME Journal of Turbomachinery, Vol. 113, pp. 42-51.

Wagner, R. and Velkoff, H., 1972, "Measurements of Secondary Flows in a Rotating Duct", ASME Journal of Engineering for Power, pp. 261-270.

Wolfstein, M., 1969, "The Velocity and Temperature Distribution of One-Dimensional Flow with Turbulence Augmentation and Pressure Gradient", International Journal of Heat and Mass Transfer, Vol 12, pp. 301-318.

Younis, B.A., 1993, "Prediction of Turbulent Flows in Rotating Rectangular Ducts", ASME Journal of Fluids Engineering, Vol 115, pp. 646-652.